Science Advances
AAAS

Supplementary Materials for

Momentum-resolved electronic structure and band offsets in an epitaxial NbN/GaN superconductor/semiconductor heterojunction

Tianlun Yu*, John Wright, Guru Khalsa, Betül Pamuk, Celesta S. Chang, Yury Matveyev, Xiaoqiang Wang, Thorsten Schmitt, Donglai Feng, David A. Muller, Huili Grace Xing, Debdeep Jena*, Vladimir N. Strocov*

*Corresponding author. Email: tianlun.yu@psi.ch (T.Y.); djena@cornell.edu (D.J.); vladimir.strocov@psi.ch (V.N.S.)

Published 22 December 2021, *Sci. Adv.* **7**, eabi5833 (2021)
DOI: 10.1126/sciadv.abi5833

This PDF file includes:

Element and orbital projected band calculations

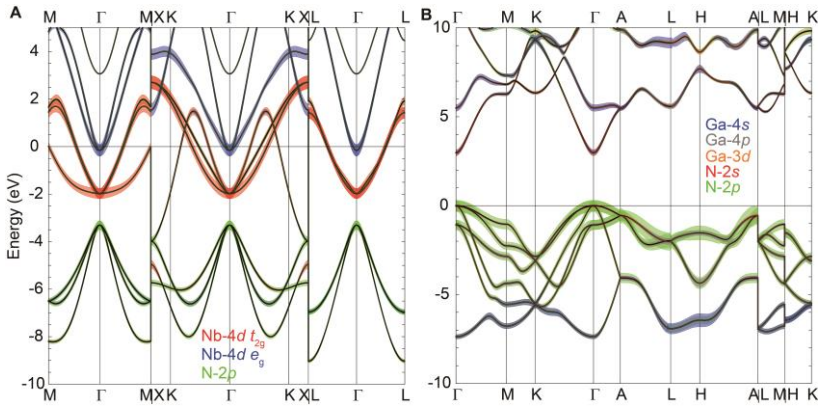

Fig. S1: **Orbitally projected band structure from DFT.** (A) The calculation results for NbN. (B) The calculation results for GaN. The width of the bands represents the amount of orbital character shown in the color-coded legend.

Orbital character of the conduction band of NbN vs polarization dependence

In our experimental geometry with NbN grown along the (111) direction, the measurement plane (including the incoming X-rays and detected photoelectrons) coincides with the Γ-K-L mirror plane (Fig. S2**A**). Then the d_{zx} orbitals of NbN, whose orbital plane is parallel to the mirror plane, form even states that are selected with *p*-polarized incident photons, while the d_{xy} and d_{yz} orbitals, inclined to the mirror plane, form degenerate even and odd linear combinations, which are selected with *p*- and *s*-polarized incident photons, respectively (Fig. S2**B**). The experimental polarization dependence (Fig. S2**C**) appears consistent with this expected behaviour of the orbital projections of the DFT bands (Fig. S2**D**) where the more dispersive band is formed by the d_{zx} orbitals and the less dispersive by the degenerate d_{xy} and d_{yz} ones. However, the unambiguous identification of the orbital character of the experimental bands is complicated by (1) the limited experimental resolution and relaxed crystallinity of the NbN film which hinder separation of the d_{zx} vs d_{xy}/d_{yz} bands; (2) the strain and again the relaxed NbN crystallinity smear the strict selection rules, calling for further thin-film growth and spectroscopic experiments. The band manifold above E_F, invisible in the experiment, is formed by the e_g x^2-y^2 and $3z^2$-r^2 orbitals (bottom panels in Fig. S2**D**). While there is qualitative agreement between the orbitally projected bands and the SX-ARPES data, quantitative details via simulation of APRES matrix elements can be explored in future studies (*58*).

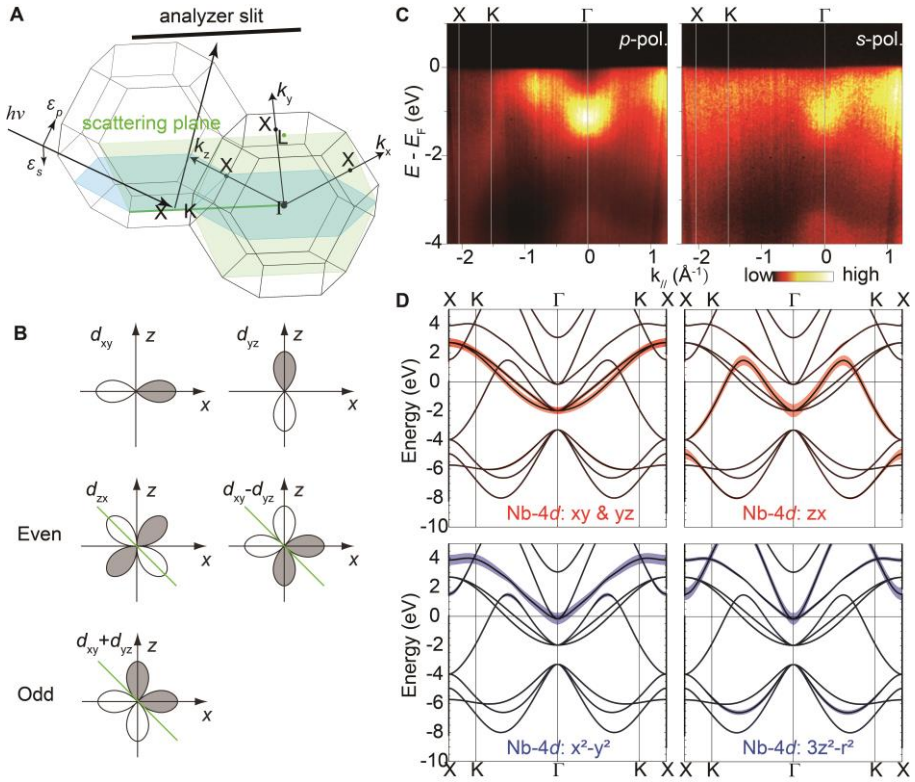

Fig. S2: **Orbital character of the conduction band of NbN.** (**A**) The BZ and the experimental scattering geometry. (**B**) The symmetry of the *d* orbitals with respect to the mirror plane (the green line) formed by the surface normal and analyzer slit. (**C**) The SX-ARPES intensity data probed with *p*- and *s*-polarized photons. (**D**) Individual projections onto the Nb-4*d* t_{2g} (*xy*,*yz*,*zx*) (top) and e_g (x^2-y^2,$3z^2$-r^2) (bottom) orbitals of NbN from DFT.

Details of the GaN experimental band structure

For GaN, fine details of the experimental spectral intensity along different directions (Fig. S3**G-R**) can be enhanced using the curvature and second-derivative representations (*59*) (Fig. S3**G-R**). For these representations, the spectral intensity was denoised by Gaussian smoothing along the energy axis with the full width of 700 meV.

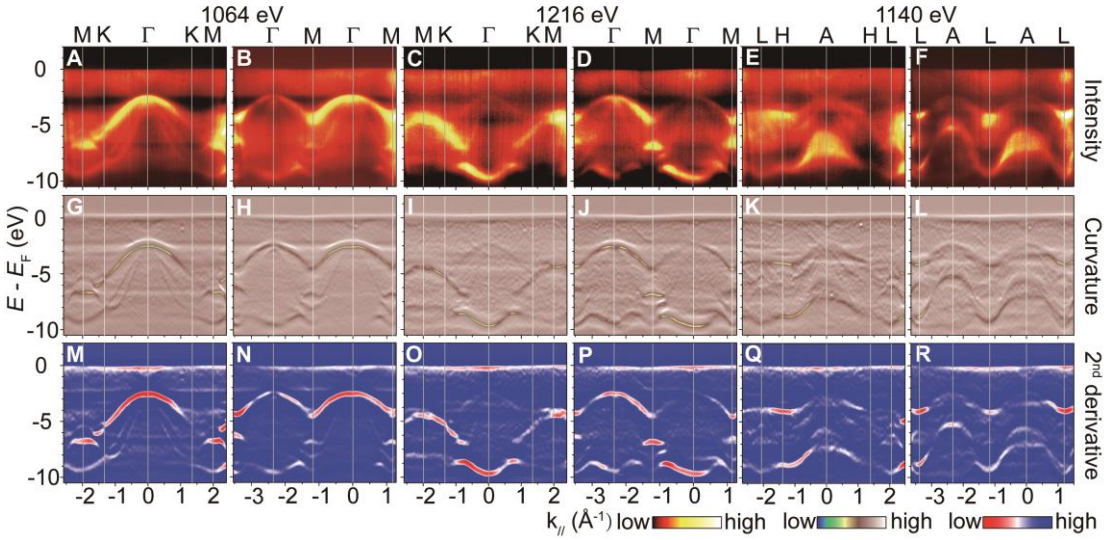

Fig. S3: **Experimental SX-ARPES results on GaN. (A-F)** The intensity images along K-Γ-K, Γ-M-Γ, H-A-H and A-L-A at different energies. **(G-L)** The corresponding curvature images. **(M-R)** The second-derivative images (positive values set to zero).

GaN band bending

The Ga 3*d* core level shows a clear energy shift as a function of *hv* between 350 eV to 1250 eV as shown in Fig. S4**A**, while the Nb 4s core level not only exhibits an approximately constant peak position, but also identical line shape. This indicates that the band bending occurs in the GaN layer, causing a shift of the Ga 3*d* peak of ~80 meV in our *hv* range (Fig. S4**B**). Using our deconvolution method as described in the Methods section, the *U*(*z*) profile was extracted based on the simple approximation $U(z) \sim z^2$ near the interface, as summarized in Fig. S4**C**, assuming that the VBM position at ~ 1 nm from the interface is equal to the experimental value -2.49 eV. Though the confidence region appears large, the determined *U*(*z*) clearly shows an upwards band bending consistent with the downward energy shift of the Ga 3*d* peak. The variation of *U*(*z*) by ~300 meV over a distance of ~6 nm from the interface is only about half of that observed in Ga-polar n-GaN (*36*), or about one third of that observed in other GaN-based heterojunctions such as GaN/AlGaN (*12*), where *U*(*z*) at the interface end is pulled down by the polarization charge, with its variation with *z* being sharpened by a high density of the mobile electrons accumulated in the interfacial quantum well. The smoothness of this *U*(z) explains why the experimental band dispersions in NbN/GaN appear significantly sharper compared to those in GaN/AlGaN measured at essentially the same *hv*.

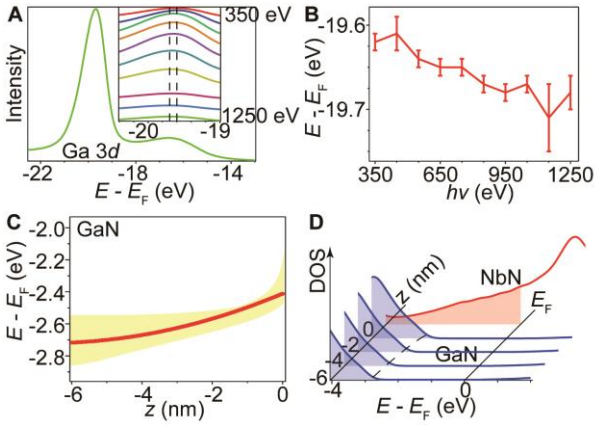

Fig. S4: **The band bending in the NbN/GaN heterojunction. (A)** The energy-dependent core level of Ga 3*d*. **(B)** The core level peak position vs *hv*. The error bar is determined by the E_F measurements before and after the core level measurement. **(C)** The depth profile of the band bending. The yellow shading represents the confidence region and the red line is the optimum profile, assuming that the VBM position at ~ 1 nm from the interface is equal to the experimental value -2.49 eV. **(D)** The bend profile of GaN/NbN heterojunction. The CBM of GaN is estimated by the calculation and the band bending profile extracted by experiments.

REFERENCES AND NOTES

1. F. Braun, Über die Stromleitung durch Schwefelmetalle. *Ann. Phys. Chem.* **153**, 556 (1874).

2. J. J. Thomson, M. A. F.R.S., XL. Cathode rays. *Lond. Edinb. Dublin Philos. Mag. J. Sci*. **44**, 293–316 (1897).

3. W. Schottky, Halbleitertheorie der Sperrschicht. *Naturwissenschaften* **26**, 843 (1938).

4. N. F. Mott, Note on the contact between a metal and an insulator or semi-conductor. *Math. Proc. Cambridge Philos. Soc*. **34**, 568–572 (1938).

5. H. A. Bethe, *Theory of the Boundary Layer of Crystal Rectifiers* (Massachusetts Institute of Technology, Radiation Laboratory, 1942).

6. A. Semenov, O. Cojocari, H. Hübers, F. Song, A. Klushin, A. Müller, Application of zero-bias quasi-optical Schottky-diode detectors for monitoring short-pulse and weak terahertz radiation. *IEEE Electron Device Lett.* **31**, 674–676 (2010).

7. R. Han, Y. Zhang, Y. Kim, D. Y. Kim, H. Shichijo, E. Afshari, K. K. O, Active terahertz imaging using Schottky diodes in CMOS: Array and 860-GHz Pixel. *IEEE J. Solid State Circuits*. **48**, 2296–2308 (2013).

8. S. Datta, III-V field-effect transistors for low power digital logic applications. *Microelectron. Eng.* **84**, 2133–2137 (2007).

9. A. F. Witulski, R. Arslanbekov, A. Raman, R. D. Schrimpf, A. L. Sternberg, K. F. Galloway, A. Javanainen, D. Grider, D. J. Lichtenwalner, B. Hull, Single-event burnout of SiC junction barrier Schottky diode high-voltage power devices. *IEEE Trans. Nucl. Sci.* **65**, 256–261 (2018).

10. A. Damascelli, Z. Hussain, Z.-X. Shen, Angle-resolved photoemission studies of the cuprate superconductors. *Rev. Mod. Phys.* **75**, 473–541 (2003).

11. M. P. Seah, W. A. Dench, Quantitative electron spectroscopy of surfaces: A standard data base for electron inelastic mean free paths in solids. *Surf. Interface Anal.* **1**, 2–11 (1979).

12. L. L. Lev, I. O. Maiboroda, M.-A. Husanu, E. S. Grichuk, N. K. Chumakov, I. S. Ezubchenko, I. A. Chernykh, X. Wang, B. Tobler, T. Schmitt, M. L. Zanaveskin, V. G. Valeyev, V. N. Strocov, k-space imaging of anisotropic 2D electron gas in GaN/GaAlN high-electron-mobility transistor heterostructures. *Nat. Commun.* **9**, 2653 (2018).

13. L. L. Lev, D. V. Averyanov, A. M. Tokmachev, F. Bisti, V. A. Rogalev, V. N. Strocov, V. G. Storchak, Band structure of the EuO/Si interface: Justification for silicon spintronics. *J. Mater. Chem. C* **5**, 192–200 (2017).

14. Y. Liu, A. Luchini, S. Martí-Sánchez, C. Koch, S. Schuwalow, S. A. Khan, T. Stankevič, S. Francoual, J. R. L. Mardegan, J. A. Krieger, V. N. Strocov, J. Stahn, C. A. F. Vaz, M. Ramakrishnan, U. Staub, K. Lefmann, G. Aeppli, J. Arbiol, P. Krogstrup, Coherent epitaxial semiconductor–ferromagnetic insulator InAs/EuS interfaces: Band alignment and magnetic structure. *ACS Appl. Mater. Interfaces* **12**, 8780–8787 (2020).

15. J. A. Krieger, Y. Ou, M. Caputo, A. Chikina, M. Döbeli, M.-A. Husanu, I. Keren, T. Prokscha, A. Suter, C.-Z. Chang, J. S. Moodera, V. N. Strocov, Z. Salman, Do topology and ferromagnetism cooperate at the EuS/Bi2Se3 interface? *Phys. Rev. B* **99**, 064423 (2019).

16. S. Schuwalow, N. B. M. Schröter, J. Gukelberger, C. Thomas, V. Strocov, J. Gamble, A. Chikina, M. Caputo, J. Krieger, G. C. Gardner, M. Troyer, G. Aeppli, M. J. Manfra, P. Krogstrup, Band structure extraction at hybrid narrow-gap semiconductor–metal interfaces. *Adv. Sci.* **8**, 2003087 (2020).

17. V. N. Strocov, L. L. Lev, M. Kobayashi, C. Cancellieri, M.-A. Husanu, A. Chikina, N. B. M. Schröter, X. Wang, J. A. Krieger, Z. Salman, k-resolved electronic structure of buried heterostructure and impurity systems by soft-x-ray ARPES. *J. Electron Spectros. Relat. Phenomena* **236**, 1–8 (2019).

18. D. Jena, R. Page, J. Casamento, P. Dang, J. Singhal, Z. Zhang, J. Wright, G. Khalsa, Y. Cho, H. G. Xing, The new nitrides: Layered, ferroelectric, magnetic, metallic and superconducting nitrides to boost the GaN photonics and electronics eco-system. *Jpn. J. Appl. Phys.* **58**, SC0801 (2019).

19. G. N. Gol'tsman, O. Okunev, G. Chulkova, A. Lipatov, A. Semenov, K. Smirnov, B. Voronov, A. Dzardanov, C. Williams, R. Sobolewski, Picosecond superconducting single-photon optical detector. *Appl. Phys. Lett.* **79**, 705–707 (2001).

20. M. Hajenius, J. J. A. Baselmans, J. R. Gao, T. M. Klapwijk, P. A. J. de Korte, B. Voronov, G. Gol'tsman, Low noise NbN superconducting hot electron bolometer mixers at 1.9 and 2.5 THz. *Supercond. Sci. Technol*. **17**, S224–S228 (2004).

21. Y. Nakamura, H. Terai, K. Inomata, T. Yamamoto, W. Qiu, Z. Wang, Superconducting qubits consisting of epitaxially grown NbN/AlN/NbN Josephson junctions. *Appl. Phys. Lett.* **99**, 212502 (2011).

22. International Roadmap for Devices and Systems (IRDS) 2017 Edition: Executive summary (2017); https://irds.ieee.org/images/files/pdf/2017/2017IRDS_ES.pdf.

23. International Roadmap For Devices and Systems (IRDS) 2020 Edition: Cryogenic electronics and quantum information processing (2020); https://irds.ieee.org/images/files/pdf/2020/2020IRDS_CEQIP.pdf.

24. G. Hägg, Eigenschaften der Phasen von Übergangselementen in binären Systemen mit Bor, Kohlenstoff und Stickstoff. *Z. Phys. Chem.* **6B**, 221 (1929).

25. R. Yan, G. Khalsa, S. Vishwanath, Y. Han, J. Wright, S. Rouvimov, D. Scott Katzer, N. Nepal, B. P. Downey, D. A. Muller, H. G. Xing, D. J. Meyer, D. Jena, GaN/NbN epitaxial semiconductor/superconductor heterostructures. *Nature* **555**, 183–189 (2018).

26. D. J. Meyer, B. P. Downey, D. Scott Katzer, N. Nepal, V. D. Wheeler, M. T. Hardy, T. J. Anderson, D. F. Storm, Epitaxial lift-off and transfer of III-N materials and devices from SiC substrates. *IEEE Trans. Semicond. Manufact*. **29**, 384–389 (2016).

27. P. Dang, G. Khalsa, C. S. Chang, D. S. Katzer, N. Nepal, B. P. Downey, V. D. Wheeler, A. Suslov, A. Xie, E. Beam, Y. Cao, C. Lee, D. A. Muller, H. G. Xing, D. J. Meyer, D. Jena, An all-epitaxial nitride heterostructure with concurrent quantum Hall effect and superconductivity. *Sci Adv*. **7**, eabf1388 (2021).

28. S. Krause, V. Mityashkin, S. Antipov, G. Gol'tsman, D. Meledin, V. Desmaris, V. Belitsky, M. Rudziński, Reduction of phonon escape time for NbN hot electron bolometers by using GaN buffer layers. *IEEE Trans. Terahertz Sci. Technol*. **7**, 53–59 (2017).

29. S. Krause, D. Meledin, V. Desmaris, A. Pavolotsky, H. Rashid, V. Belitsky, Noise and IF gain bandwidth of a balanced waveguide NbN/GaN hot electron bolometer mixer operating at 1.3 THz. *IEEE Trans. Terahertz Sci. Technol*. **8**, 365–371 (2018).

30. A. M. Witowski, K. Pakuła, J. M. Baranowski, M. L. Sadowski, P. Wyder, Electron effective mass in hexagonal GaN. *Appl. Phys. Lett.* **75**, 4154–4155 (1999).

31. L. F. Wagner, R. W. Young, A. Sugerman, A note on the correlation between the Schottky-diode barrier height and the ideality factor as determined from I-V measurements. *IEEE Electron Device Lett.* **4**, 320–322 (1983).

32. A. Semenov, B. Günther, U. Böttger, H.-W. Hübers, H. Bartolf, A. Engel, A. Schilling, K. Ilin, M. Siegel, R. Schneider, D. Gerthsen, N. A. Gippius, Optical and transport properties of ultrathin NbN films and nanostructures. *Phys. Rev. B* **80**, 054510 (2009).

33. L. Toth, *Transition Metal Carbides and Nitrides* (Elsevier, 2014).

34. F. Weber, R. Hott, R. Heid, L. L. Lev, M. Caputo, T. Schmitt, V. N. Strocov, Three-dimensional Fermi surface of 2*H*−NbSe2: Implications for the mechanism of charge density waves. *Phys. Rev. B* **97**, 235122 (2018).

35. V. N. Strocov, Intrinsic accuracy in 3-dimensional photoemission band mapping. *J. Electron Spectrosc. Relat. Phenom.* **130**, 65–78 (2003).

36. Y. Zhao, H. Gao, R. Huang, Z. Huang, F. Li, J. Feng, Q. Sun, A. Dingsun, H. Yang, Precise determination of surface band bending in Ga-polar n-GaN films by angular dependent x-ray photoemission spectroscopy. *Sci. Rep.* **9**, 16969 (2019).

37. P. D. C. King, T. D. Veal, C. E. Kendrick, L. R. Bailey, S. M. Durbin, C. F. McConville, InN/GaN valence band offset: High-resolution x-ray photoemission spectroscopy measurements. *Phys. Rev. B* **78**, 033308 (2008).

38. J. R. Waldrop, R. W. Grant, Measurement of AlN/GaN (0001) heterojunction band offsets by x-ray photoemission spectroscopy. *Appl. Phys. Lett.* **68**, 2879–2881 (1996).

39. S. W. King, R. J. Nemanich, R. F. Davis, Band alignment at AlN/Si (111) and (001) interfaces. *J. Appl. Phys.* **118**, 045304 (2015).

40. J. J. Lee, F. T. Schmitt, R. G. Moore, S. Johnston, Y. T. Cui, W. Li, M. Yi, Z. K. Liu, M. Hashimoto, Y. Zhang, D. H. Lu, T. P. Devereaux, D.-H. Lee, Z.-X. Shen, Interfacial mode coupling as the origin of the enhancement of Tc in FeSe films on $SrTiO_3$. *Nature* **515**, 245–248 (2014).

41. Q. Song, T. L. Yu, X. Lou, B. P. Xie, H. C. Xu, C. H. P. Wen, Q. Yao, S. Y. Zhang, X. T. Zhu, J. D. Guo, R. Peng, D. L. Feng, Evidence of cooperative effect on the enhanced superconducting transition temperature at the FeSe/$SrTiO_3$ interface. *Nat. Commun.* **10**, 758 (2019).

42. C. Verdi, F. Caruso, F. Giustino, Origin of the crossover from polarons to Fermi liquids in transition metal oxides. *Nat. Commun.* **8**, 15769 (2017).

43. C. Cancellieri, A. S. Mishchenko, U. Aschauer, A. Filippetti, C. Faber, O. S. Barišić, V. A. Rogalev, T. Schmitt, N. Nagaosa, V. N. Strocov, Polaronic metal state at the $LaAlO_3/SrTiO_3$ interface. *Nat. Commun.* **7**, 10386 (2016).

44. V. Y. Davydov, Y. E. Kitaev, I. N. Goncharuk, A. N. Smirnov, J. Graul, O. Semchinova, D. Uffmann, M. B. Smirnov, A. P. Mirgorodsky, R. A. Evarestov, Phonon dispersion and Raman scattering in hexagonal GaN and AlN. *Phys. Rev. B* **58**, 12899–12907 (1998).

45. C. H. P. Wen, H. C. Xu, Q. Yao, R. Peng, X. H. Niu, Q. Y. Chen, Z. T. Liu, D. W. Shen, Q. Song, X. Lou, Y. F. Fang, X. S. Liu, Y. H. Song, Y. J. Jiao, T. F. Duan, H. H. Wen, P. Dudin, G. Kotliar, Z. P. Yin, D. L. Feng, Unveiling the superconducting mechanism of $Ba_{0.51}K_{0.49}BiO_3$. *Phys. Rev. Lett.* **121**, 117002 (2018).

46. K. Horiba, M. Kitamura, K. Yoshimatsu, M. Minohara, E. Sakai, M. Kobayashi, A. Fujimori, H. Kumigashira, Isotropic kink and quasiparticle excitations in the three-dimensional perovskite manganite $La_{0.6}Sr_{0.4}MnO_3$. *Phys. Rev. Lett.* **116**, 076401 (2016).

47. R. Cheng, J. Wright, H. G. Xing, D. Jena, H. X. Tang, Epitaxial niobium nitride superconducting nanowire single-photon detectors. *Appl. Phys. Lett.* **117**, 132601 (2020).

48. V. N. Strocov, X. Wang, M. Shi, M. Kobayashi, J. Krempasky, C. Hess, T. Schmitt, L. Patthey, Soft-x-ray ARPES facility at the ADRESS beamline of the SLS: Concepts, technical realisation and scientific applications. *J. Synchrotron Radiat.* **21**, 32–44 (2014).

49. V. N. Strocov, T. Schmitt, U. Flechsig, T. Schmidt, A. Imhof, Q. Chen, J. Raabe, R. Betemps, D. Zimoch, J. Krempasky, X. Wang, M. Grioni, A. Piazzalunga, L. Patthey, High-resolution soft x-ray beamline ADRESS at the Swiss Light Source for resonant inelastic x-ray scattering and angle-resolved photoelectron spectroscopies. *J. Synchrotron Radiat*. **17**, 631–643 (2010).

50. J. Braun, J. Minár, S. Mankovsky, V. N. Strocov, N. B. Brookes, L. Plucinski, C. M. Schneider, C. S. Fadley, H. Ebert, Exploring the XPS limit in soft and hard x-ray angle-resolved photoemission using a temperature-dependent one-step theory. *Phys. Rev. B* **88**, 205409 (2013).

51. G. Kresse, J. Furthmüller, Efficient iterative schemes for ab initio total-energy calculations using a plane-wave basis set. *Phys. Rev. B* **54**, 11169–11186 (1996).

52. G. Kresse, D. Joubert, From ultrasoft pseudopotentials to the projector augmented-wave method. *Phys. Rev. B* **59**, 1758–1775 (1999).

53. J. P. Perdew, K. Burke, M. Ernzerhof, Generalized gradient approximation made simple. *Phys. Rev. Lett.* **77**, 3865–3868 (1996).

54. A. V. Krukau, O. A. Vydrov, A. F. Izmaylov, G. E. Scuseria, Influence of the exchange screening parameter on the performance of screened hybrid functionals. *J. Chem. Phys.* **125**, 224106 (2006).

55. Y. A. Matveyev, A. M. Markeev, Y. Y. Lebedinskii, A. A. Chouprik, K. V. Egorov, W. Drube, A. V.

Zenkevich, Resistive switching effect in HfxAl-xOy with a graded Al depth profile studied by hard x-ray photoelectron spectroscopy. *Thin Solid Films* **563**, 20–23 (2014).

56. Y. Matveyev, D. Negrov, A. Chernikova, Y. Lebedinskii, R. Kirtaev, S. Zarubin, E. Suvorova, A. Gloskovskii, A. Zenkevich, Effect of polarization reversal in ferroelectric TiN/$Hf_{0.5}Zr_{0.5}O_2$/TiN devices on electronic conditions at interfaces studied in operando by hard x-ray photoemission spectroscopy. *ACS Appl. Mater. Interfaces* **9**, 43370–43376 (2017).

57. S. Tanuma, C. J. Powell, D. R. Penn, Calculations of electron inelastic mean free paths. V. Data for 14 organic compounds over the 50–2000 eV range. *Surf. Interface Anal.* **21**, 165–176 (1994).

58. R. P. Day, B. Zwartsenberg, I. S. Elfimov, A. Damascelli, Computational framework chinook for angle-resolved photoemission spectroscopy. *npj Quant. Mater*. **4**, 54 (2019).

59. Y. He, Y. Wang, Z.-X. Shen, Visualizing dispersive features in 2D image via minimum gradient method. *Rev. Sci. Instrum.* **88**, 073903 (2017).